NeuroImage 207 (2020) 116354

Contents lists available at ScienceDirect

NeuroImage

journal homepage: www.elsevier.com/locate/neuroimage

The small scale functional topology of movement control: Hierarchical organization of local activity anticipates movement generation in the premotor cortex of primates

Giampiero Bardella [a,b,1], Pierpaolo Pani [b,1], Emiliano Brunamonti [b], Franco Giarrocco [a,b], Stefano Ferraina [b,*]

[a] PhD Program in Behavioral Neuroscience, Sapienza University of Rome, Italy
[b] Department of Physiology and Pharmacology, Sapienza University of Rome, Piazzale Aldo Moro 5, 00185, Rome, Italy

ARTICLE INFO

Keywords:
Movement control
Premotor cortex
Functional topology
Countermanding task

ABSTRACT

How neurons coordinate their collective activity for behavioural control is an open question in neuroscience. Several studies have progressively proven, on various scales, that the patterns of neural synchronization change accordingly with behavioural events. However, the topological features of the neural dynamics that underlie task-based cognitive decisions on the small scale level are not understood. We analysed the multiunit activity (MUA) from a multielectrode (96 channels) array of the dorsal premotor cortex (PMd) in rhesus monkeys during a countermanding reaching task. Within the framework of graph theory, we found that in the local PMd network motor execution is preceded by the emergence of hubs of anti-correlation that are organized in a hierarchical manner. Conversely, this organization is absent when monkeys correctly inhibit programmed movements. Thus, we interpret the presence of hubs as reflecting the readiness of the motor plan and the irrevocable signature of the onset of the incoming movement.

1. Introduction

Billions of interconnected neurons that propagate signals rapidly over short and long distances form the brain. Their interactions have been examined by two approaches: on a small scale, aiming to describe how relatively few individual neurons cooperate in a given area, using in vitro or in vivo models, and a large scale, characterizing how large populations of neurons, from different macro areas, are functionally connected. The small-scale approach has been used, for example, to examine areas of the cortico-subcortical network, which underlies the control and generation of skilled arm movements. However, for many years, neural activity has been recorded from few neurons, with limited efforts to extract a population code that can account for the interactions between neurons (Evarts, 1968; Georgopoulos et al., 1989; Wise et al., 1997). Recently, the diffusion of high-density multi-electrode arrays has made it possible to adequately study local population dynamics, thanks to the ability of simultaneously recording tens to hundreds of neurons. Using various forms of reduction complexity, the population activity in cortical motor areas has been described as a neural trajectory as a function of time, evolving in a multidimensional neuronal state space (Gallego et al., 2017; Churchland et al., 2012; Shenoy et al., 2012). These approaches, particularly when they are used to study cognitively advanced functions, have provided valuable information on how small populations of neurons cooperate during decisions, movement planning and execution. In parallel, other studies have found that simultaneously recorded neurons can display functional coupling (spike synchronization), even without undergoing any modulation in their firing rate (Fetz, 1992). Neuronal synchronization patterns change, depending on behavioural events (Vaadia et al., 1988; Hatsopoulos et al., 1998; Riehle et al., 1997; Torre, 2016), even independent of the underlying oscillatory pattern of activation (Fujisawa et al., 2008). On a larger scale, neuronal synchronization has been analysed to examine the level of interaction between areas of the entire brain network (Konig and Engel, 1995; Michaels et al., 2016). Several methods that focus on human electroencephalography (EEG) and functional-MRI (fMRI) data (Shin et al., 2013; Demuru et al., 2013; Luca et al., 2006; Liégeois et al., 2014; Bordier et al., 2018; Nicolini et al., 2017) have been successfully applied. With these approaches, analytical techniques that are derived from graph theory have shown that

* Corresponding author.
E-mail address: stefano.ferraina@uniroma1.it (S. Ferraina).
[1] Equally contributed.

https://doi.org/10.1016/j.neuroimage.2019.116354
Received 11 August 2019; Received in revised form 24 October 2019; Accepted 11 November 2019
Available online 16 November 2019

neuronal population interactions are organized according to a highly efficient topology, with local and long-distance connections occasionally organised around highly functionally coupled regions (Power et al., 2013; Lutcke et al., 2013; Eguiluz et al., 2005; Vlasov and Bifone, 2017; Mastrandrea et al., 2017). Conversely, graph-based approaches have been used sparingly on data from animal models, with few exceptions (Sporns et al., 2007; Gu et al., 2019; Yu et al., 2006; Dann et al., 2016; Kiani et al., 2015; Gerhard et al., 2011; Ferraro et al., 2018; Gal et al., 2013) and, to our knowledge, not at all to describe the dynamics of local functional connectivity structures in vivo on a small scale. Thus, we wanted to study the local functional connectivity of the dorsal premotor cortex (PMd) in monkeys, preceding motor execution. We focused on the spectral estimate of the multiunit activity (MUA) signal (Mattia et al., 2013), obtained from a 96-channel array. To increase our understanding of the topology of the network, we used a percolation-based approach (Bordier et al., 2017, 2018; Nicolini et al., 2017; Vlasov and Bifone, 2017; Mastrandrea et al., 2017; Ferraro et al., 2018; Callaway et al., 2000; Gallos et al., 2012). Percolation is a powerful tool that is derived from statistical physics that allows one to inspect the self-organization of networks. Our study shows that the PMd exhibits signatures of self-organization only when the motor plan is mature, not when it is successfully cancelled. Further, the occurrence of this phenomenon correlates with the emergence of functional hubs in the network.

2. Results

2.1. Behavioural evaluation of the lead time to suppress a movement

To examine the local functional connectivity before movement execution, we recorded neuronal activity from the PMd of two monkeys (P, C) that were performing a countermanding reaching task (Fig. 1). At the beginning of the task, the animals were required to hold their hand over a central target that was presented on a touch screen. Two types of randomly intermingled trials were possible: no-stop trials (67%) and stop trials (33%). During no-stop trials, concurrent with the disappearance of the central target (Go signal), a peripheral target appeared on the left or right. To obtain the reward, the monkeys were instructed to reach the peripheral target. In stop trials, after the Go signal, the central target reappeared (Stop signal) after a variable delay, called the SSD (Stop signal Delay). The monkeys were then required to refrain from moving to earn the reward. If the movement is withheld, the trial is a stop-correct trial; otherwise, it is a stop-wrong trial. Generally in these trials the monkeys detached the hand from the screen and then stopped the movement on the fly avoiding to touch the peripheral target. Immediately after the error a blank screen was displayed. Typically, in relation to the duration of the average SSD, the stop-correct trials constituted approximately 50% of stop trials.

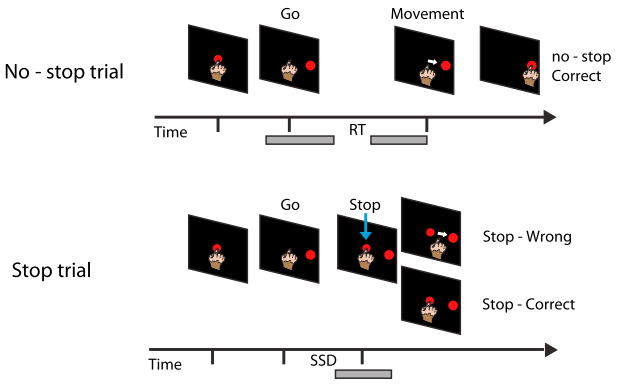

Fig. 1. Behavioural task and epochs of analysis. No-stop and stop trials were randomly intermixed during each session. The gray horizontal rectangles under the time scale of no-stop and stop trials represent the epochs of analysis (Go epoch, Pre-Movement epoch, Stop signal epoch, respectively). RT reaction time; SSD Stop signal delay.

The countermanding task permits one to inspect the neuronal correlates of movement execution by comparing trials in which movements are planned and then executed (no-stop trials) with those in which movements are planned and then aborted (stop-correct trials). In this comparison, it is ideal to identify the specific neuronal signature of the movement execution and determine when it occurs. Moreover, it allows one to establish when the neuronal signature that is specific for movement execution must manifest. The countermanding task makes it possible to calculate a behavioural measure that it is broadly considered an index of efficiency in movement suppression: the stop signal reaction time or SSRT. To estimate SSRT the race model (Logan et al., 1984) must be applied. This model describes the behaviour in the stop trials as the result of two stochastic processes racing toward a threshold: the GO process triggered by the onset of the Go signal, which duration is represented by the RT, and the STOP process triggered by the onset of the Stop signal, which duration must be calculated. When the GO process wins the race the movement is generated (stop-wrong trial), alternatively it is withheld (stop-correct trials). The race model allows to estimate the SSRT by taking into account the duration of the GO process, the probability to respond, and the SSDs. However to make the race model applicable to study response inhibition, a central assumption must be satisfied: the GO process in the stop trials must be the same as in the no-stop trials (independence assumption). Indeed the RTs that are employed to estimate the SSRT are obtained from the no-stop trials. To broadly validate this assumption, stop-wrong RTs must be shorter than the no-stop trials (Logan et al., 1984) (see Table 1). To estimate the SSRT we employed the integration method because it has been proven to be the most reliable (Band et al., 2003). It assumes that the finishing time of the Stop process corresponds to the nth no-stop RT, where n results from the multiplication of the ordered no-stop RTs distribution by the overall probability of responding, p(respond). The SSRT is then obtained by subtracting the average SSD from the nth no-stop RT. The SSRT can also be considered the lead time that is required to inhibit a movement, or, simply, the time that precedes the start of a movement when a Stop signal, if presented, halts the generation of the same movement approximately 50% of the time. If the Stop signal is presented after this time, it will be less effective, because the neuronal phenomena that lead to the movement generation will have already started. If the Stop signal is presented well before this time, it will be more effective in halting the movement. Consequently, the neuronal activity that is related to movement generation must occur around the time that is defined by the SSRT before the movement onset.

2.2. In the PMd, certain recording sites show anti-correlated neuronal activity before movement generation

We focused on no-stop trials, i.e., the trials that required movement generation—to examine the organization of the functional network in the PMd in relation to movement execution. Consistent with previous approaches that have shown that important changes in single and multiunit activities and local field potentials occur in the PMd in the time before movement onset, (Mattia et al., 2013, 2010; Kaufman et al., 2016; Pani et al., 2014; Lara et al., 2018; Chandrasekaran et al., 2014), Fig. 2 shows

Table 1
Behavioural results. For each monkey mean and standard deviation are presented for RTs in no-stop (RT_{ns}) and stop-wrong (RT_{sw}) trials, and presented SSDs. The estimates of SSRT were obtained after checking for the statistical difference (Independence assumption; rank-sum test) between RT_{ns} and RT_{sw}.

Monkeys	RT_{ns}	RT_{sw}	SSD	SSRT	Independence test	P(r)
P	769 (110)	710 (82)	557 (115)	203	P = 8.44 e−5; zval −3.9; ranksum = 7411	0.48
C	585 (92)	537 (71)	371 (110)	190	P = 8.58 e−5; zval −3.9; ranksum = 9213	0.44

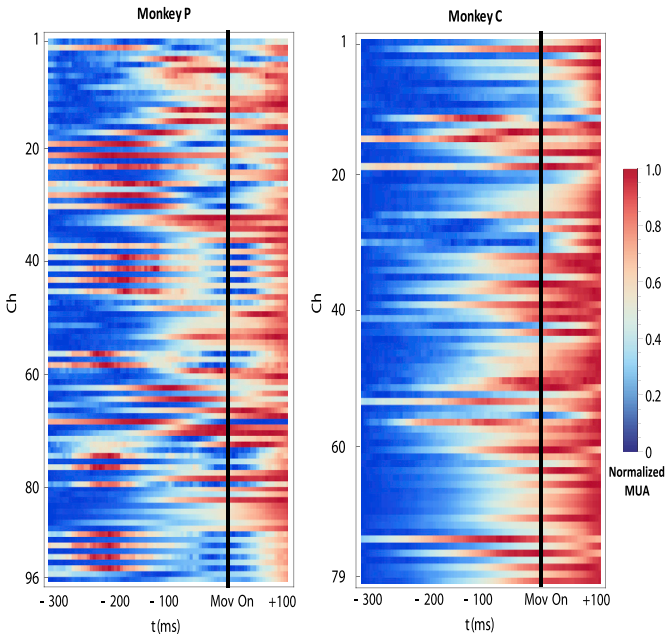

Fig. 2. Trial-averaged single channel MUA aligned to the movement onset. Normalised MUA (no-stop trials) for every single recording channel in the two animals. Broken electrodes have been removed from the list in Monkey C.

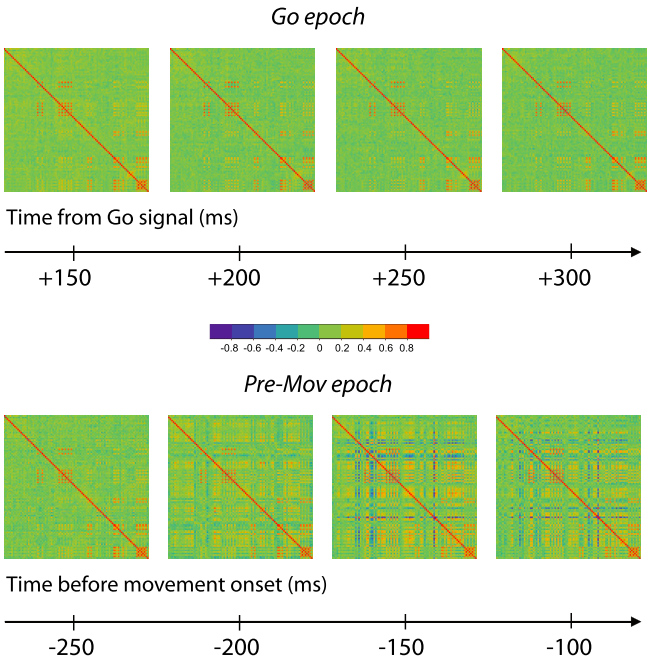

Fig. 3. Average network series changes during RT. Snapshots of the average network time series at four different times from the Go (Go; top) and before the movement (Pre-mov; bottom) epochs of no-stop trials in monkey P. The scale bar indicates the values of correlation coefficients.

that most of the recording sites in the arrays were modulated, demonstrating increased or decreased MUA activity, in the 300 ms that preceded the movement onset. We have suggested (Mattia et al., 2013) that these changes constitute a signature of the maturation of the motor plan, achieved in cortical modules that show both positive (low-to-high) and negative (high-to-low) transitions in the MUA.

We examined the level of mutual interactions among various recording sites by computing a correlation matrix between MUA time series using a sliding window approach. We modelled the evolving interactions of the network as a sequence of snapshots of correlation matrices, at the single-trial (single-trial network time series) and average levels (average network time series; see 4 for further details). Within this framework, each recording site can be considered a node of the functional network in the PMd, and the connections (or links) represent the amount of interaction (synchrony) between nodes. In our case, the weight of each connection was the correlation coefficient between corresponding time series. Notably, certain recording channels had a negative median value of the distribution of correlation coefficients in the 200 ms that preceded the movement onset (Supplementary Fig. S1), suggesting the presence of nodes with specific functions in the PMd network of both monkeys. Fig. 3 (and Supplementary Fig. S2, for the other animal) shows selected snapshots of the average network time series aligned to the Go signal (top) and movement onset (bottom) in Monkey P. We found that although nothing peculiar occurred after the Go signal (Go epoch) as the time of movement generation approached (Pre-Movement epoch), positive (red regions) and negative correlations (blue regions) appeared. The marked blue lines (nodes that anti-correlate with the rest of the network) suggest that the network is more organized in the selected snapshots and that the anti-correlation is a determinant of this functional change.

2.3. In the functional network of the PMd, a hierarchy of hubs of anti-correlation emerges before movement generation

To quantitatively assess whether the emergence of negative correlations is the signature of the impending movement generation and to monitor the evolution of the network configurations, we performed dynamic percolation analysis. This technique allows one to inspect the network organization by iteratively removing links between nodes as a function of a control parameter. As a control parameter, which quantifies the structural characteristics of the network, we used the number of connected clusters of nodes in the network (Bardella et al., 2016) (namely, the number of connected components; see 4 for further details). The results of the percolation are encoded in a percolation curve, in which the number of connected components is plotted as a function of a threshold (i.e., the link weights). Thus, link weights represent the thresholds according to which network disintegration is monitored. Moreover, because links are removed based on the value of their weights this process reveals the presence of a hierarchical organization within the network. If the network is randomly arranged at the time of analysis, the curve is characterized by a sharp transition in the number of connected components for changes in threshold values. Thus, the network disintegrates very quickly on removal of the links, and there are no stable configurations of its constituent components. Conversely, when a hierarchical structure is present, for certain threshold values, stable clusters of nodes (number of connected components) exist, and the network is insensitive to the progressive removal of links. This yields a stepwise percolation curve in which plateaus reflect the presence of stable hierarchical configurations in the network. Fig. 4 shows the percolation curves (step: 5 ms; see 4) for negative correlations of no-stop trials, separately for each animal, starting from 300 ms before movement onset.

In the early phase (light blue lines), the curves are characterized by the absence of plateaus and by steep transitions in the number of connected components. Later (at different times in the two animals; darker lines), the trends become more stepwise. This pattern suggests that, approaching the movement onset, the functional network of anti-correlations of the PMd evolves from a pseudo-random state toward a more organized state that is endowed with signatures of hierarchy. We calculated the slope of all percolation curves that were obtained and plotted them as a function of time (Fig. 5, A) to generate a straightforward view of the evolution from pseudo-random to organized state in the pre-Movement epoch for both animals. We found that at approximately 200 ms before the movement in both animals, a transition in the average slope appeared (from roughly −600 to −200). To validate the results of the percolation analysis statistically, we proposed a null model (see 4)

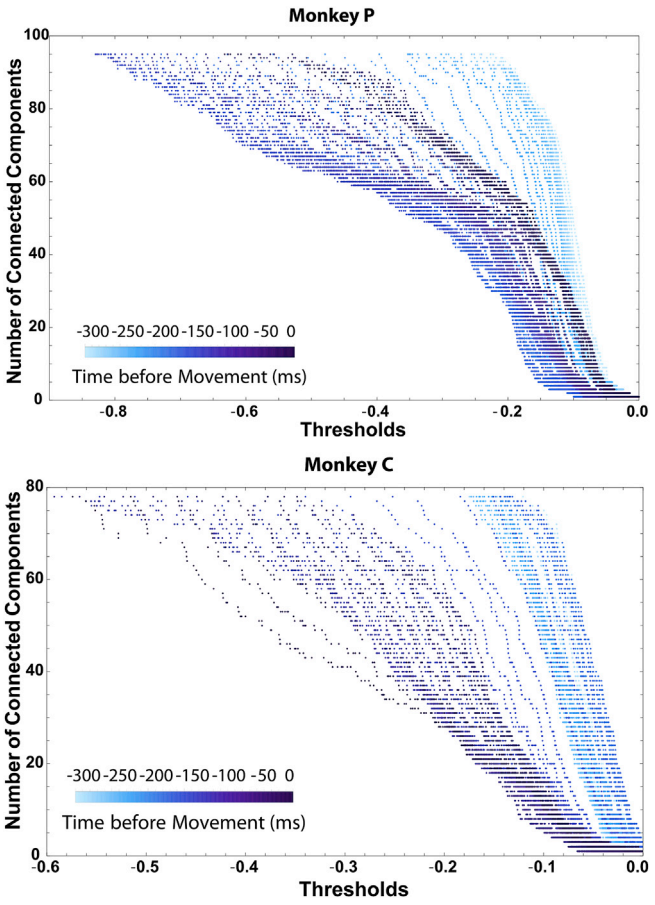

Fig. 4. Percolation curves before Movement onset in no-stop trials. Time evolution of the percolation curves for 300 ms before the movement onset, for each monkey. Times far from the movement onset are coloured in lighter shades of blue and times close to the movement onset in darker shades of blue. Thresholds values are correlation coefficients.

and computed the slope of each percolation curve for the experimental data and null model. We expected the experimental trend to be reproduced by the null model during the early stages of the epoch and to differ significantly when approaching the later stages. The results show that the steepness of the percolation curve did not differ significantly from the null model for times that were far from the movement onset (Fig. 5B, top), whereas it lay well outside of the 95% confidence interval in the late stages (Fig. 5 B, bottom).

To obtain the complete picture of the network evolution, we examined its topology in greater detail, searching for a measure of available functional connections for each node and for the presence of hubs. In percolation, the threshold immediately prior to the beginning of network disintegration (disintegration starts when the number of connected components is > 1 for the first time) is critical. Indeed, recent studies (Nicolini et al., 2017; Bordier et al., 2017) have demonstrated that at this threshold, the optimal balance between information about network organization and statistical noise is realized (see 4 for further details). Thus, we inspected the network topology at this threshold and found that nodes with links (measured as Vertex Degree; VD; see 4) that greatly exceeded the average value existed (see Supplementary Fig. S3), consistent with the definition of hub nodes (Albert and Barabasi, 2002). Hubs are, indeed, the most important nodes in the network and, during percolation, preserve high VD values at high thresholds. Inspecting the entire sequence of thresholds — that is, climbing the ladder of the percolation curve — we unfolded the stable configurations of the network, and a hierarchy of hubs was revealed. Supplementary Fig. S4 shows the configuration (hubs are colour-coded) for four threshold values for Monkeys P and C before the movement onset.

2.4. Network dynamics when movements are cancelled

Supplementary Fig. S5 shows the percolation curves and the evolution of the percolation slopes for stop-wrong trials in the pre-movement epoch. The comparison with Figs. 4 and 5 suggests that the network evolves very similarly in no-stop and stop-wrong trials. At this stage, a natural question arises: what happens to the network functional structure during stop-correct trials? If the emergence of the observed hubs is a mark of the incoming movement onset, it should be absent in stop-correct trials, when the movement execution is aborted. To this end, as we did for no-stop trials, we performed percolation analysis on the average network time series, relative to (from 100 ms before to 100 ms after) the Stop signal, for stop-wrong and stop-correct trials (see Supplementary Fig. S6), calculating the corresponding slopes (Fig. 6, top). To determine whether a difference in the configurations of the network between conditions existed, we computed the Euclidean distance between all slope values. We found that the maximum distance was reached approximately 25 ms before the Stop signal presentation — as a consequence of the decreasing slope values in stop-correct trials — for both animals.

Then, we compared the network states of stop-wrong trials to those of stop-correct trials and found that during stop-correct trials, hubs were absent while emerged in stop-wrong trials (Supplementary Fig. S7), confirming the link between the emergence of hubs and movement generation. Moreover, the hubs channels were the same in stop-wrong and no-stop trials. Despite the sketch suggests an intriguing specific location for the hubs in the brain region, we avoided to link our observations to anatomical landmarks. The issue deserves future investigation.

To validate the main finding in Fig. 6 top, we tested our results against the null model (Fig. 6, bottom), averaging the correlation matrices of the average network time series that corresponded to the interval $[-50, +50]$ ms with respect to the Stop-signal (it fully contains the point of maximum distance between slopes). We then compared the experimental slope with those that were obtained from the randomization. As reported in Fig. 6, the slope of the observed percolation curve for stop-wrong trials was outside of the 95% confidence interval of the null distribution for both animals. For stop-correct trials, we found that Monkey P had a slope that was well inside of the distribution of randomizations, thus confirming the hypothesis that the network is maintained in a pseudo-random configuration. For Monkey C, the slope was still reproduced by the null model but was closer to the 95% confidence interval compared with Monkey P. However, the absence of hubs led us to conclude that the state that the network expresses during a stop-correct trial is a sort of a quiescent configuration, in which the motor plan is not fully mature and thus cannot become a movement, because no hubs take the lead. If, in that window, the hubs become active, the Stop signal, even if it is presented, is ineffective. We believe that the emergence of hubs is proof of spontaneous self-reorganization of the network from a pseudo-random to more organized state in light of a forthcoming cognitive decision (moving vs not moving).

2.5. Topology of the functional network of the PMd before executed and cancelled movements

To complement the percolation results, we implemented an increasingly used technique in neuroscience: minimum spanning tree analysis (MST; Stam et al., 2014; see 4 for further details). For a given graph, MST provides a unique connected graph without cycles or loops. MST corresponds to a subnetwork, the links of which are the strongest within the set of all possible ones. MST identifies the core structure of a network and, for this study, elicits the backbone of functional connectivity of the PMd. Two extreme configurations are possible, as quantified by Leaf Number (LN; see 4 for further details), for the MST (Stam et al., 2014): star-like, in which one (or more) central node is connected to all others via one link only, and chain-like, in which all nodes (with the exception

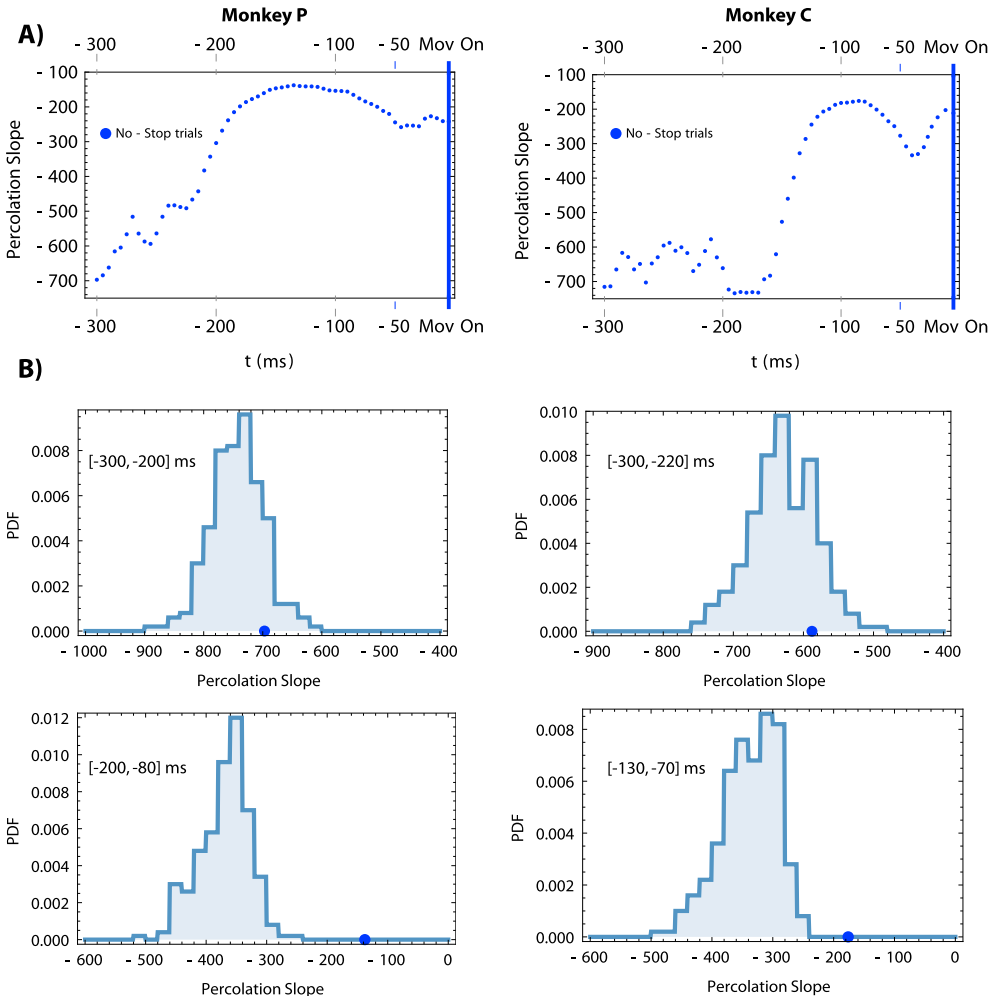

Fig. 5. Dynamics of the percolation slopes before movement onset and comparison with null models in two sub-epochs. A) Evolution of the slope of the percolation curves during the pre-movement epoch. B) Comparison with the null model for the early (top) and the late (bottom) phases of the epoch. For the early stages we averaged the matrices of the average network time series corresponding to the interval [-300,-200] ms for monkey P and [-300, −220] ms for monkey C. For the late stages we averaged the matrices of the average network time series corresponding to the interval [-200, −80] ms for monkey P and [-130, −70] ms for monkey C. Histograms: null model data. Blue dots represent the experimental slopes obtained for each interval. PDF, probability density function.

of the extremes) are connected to two others (see 4 for further details). In the first scenario, the central nodes are the hubs of the network. In the latter, the MST stretches out, with hubs excluded. Fig. 7 (and Supplementary Fig. S 8, for Monkey C) shows the results of the MST analysis for the average network time series for no-stop (before the Movement onset) and stop-wrong/correct trials (at the time of the appearance of the Stop signal). To correctly compare no-stop trials and stop-wrong trials, an equivalent time T with respect to the movement onset in both trials must be chosen. To this end we derived a time T — as an estimate of the Stop signal appearance — for the no-stop trials as: $T = \overline{RT}_{sw}\text{-}\overline{SSD}_{sw}$, where $\overline{RT}_{sw}$ is the mean reaction time for the stop-wrong trials and $\overline{SSD}_{sw}$ is the mean Stop signal delay in stop-wrong trials.

The dynamics of the MST in the Pre-mov epoch is shown in the Supplementary Video V1 (for Monkey P) and Supplementary Video V2 (for monkey C). MST was computed every 20 ms (in the interval -300 -60 ms before movement onset). Videos show the gradual evolution in the configurations, from chain to star, as the movement time is approaching.

Although multiple hubs (green circles) are evident in no-stop trials and stop-wrong trials, they are absent in stop-correct trials where MST configuration is more chain-like, as expected. To determine the statistical significance of the findings, we used the corresponding null model (Supplementary Fig. S9). The results show that during no-stop and stop-wrong trials (blue and red dots), the star-like topology (average LN) of the MST was not reproduced by the null model. During stop-correct trials (green dots), the MST configuration of Monkey P was reproduced by the ensemble of randomizations, whereas for Monkey C, it was close to the 95% confidence interval. In both cases, the hubs nodes that were characteristic of no-stop and stop-wrong trials were absent, consistent with what was found by percolation analysis and confirming that during stop-correct trials, the network lies in a meta-state at the borders of randomness and is not fully mature (i.e., not organized).

To check for the stability of the functional structure observed we repeated the same analysis in one of the other available sessions with similar characteristics. The session was recorded about 9 months apart in monkey P. The results show that the described features in MUA modulation are stable, i.e., a hierarchical organized pattern of anticorrelation emerges before movement onset, together with the star like topology and hubs (see Supplementary Fig. S10, top). Similar features have been observed in other sessions (not shown). However, we were not able to detect the same functional organization by analyzing single units extracted (see 4) from the same session (see Supplementary Fig. S10, bottom).

2.6. *Characterization of network of positive correlations*

We also applied percolation analysis to the network of positive correlations, finding that its topology was less informative than that of negative correlations because does not show presence of hubs organized in a hierarchical manner. Except for the presence of the hubs that had already been identified in the analysis of negative correlations, we failed to observe other specific topological signatures (e.g., the VD distributions shows no evidence of hubs; see Supplementary Fig. S11). Further, we found that the hubs of anti-correlation shared high positive correlation values within themselves, forming the most important cluster in the network of positive correlations. By percolation analysis, we monitored

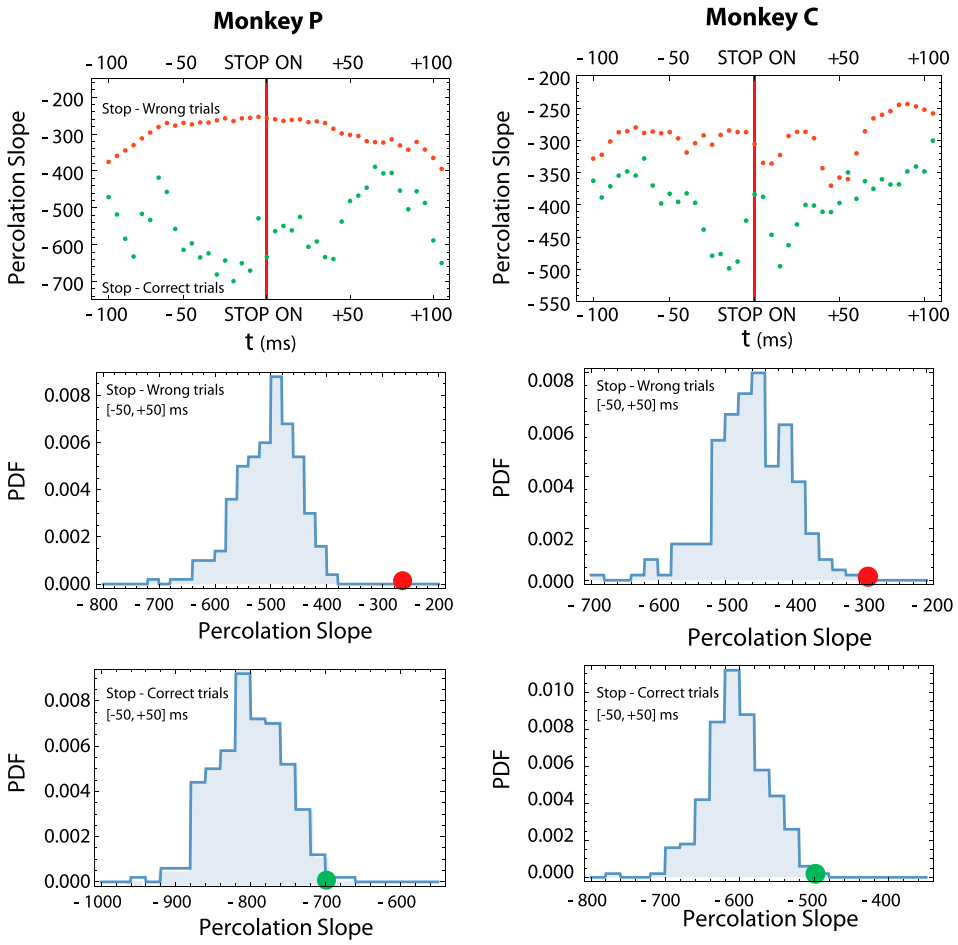

Fig. 6. Percolation curves dynamics in stop trials. Top panels: evolution of the experimental slope of the percolation curve during the epoch for stop-wrong trials (red) and stop-correct trials (green). Bottom panels: comparison between the observed slope (coloured dots; red stop-wrong trials, green stop-correct trials) and the corresponding null models (histograms). The red vertical line marks the Stop signal presentation. Other conventions and symbols as in Fig. 5.

the decomposition of this cluster (see Supplementary Fig. S12) concluding that the hubs of anti-correlation form a sort of 'rich-club' (Colizza et al., 2006), in which the links between hubs are positive (see Supplementary Fig. S13). These results show that the dynamic of the functional network of the PMd relies on the coordinated action of a small subset of neuronal populations that synchronously anti-synchronize with the rest of the network. This finding also suggests that the most notable features regarding the topological arrangement of the network are encoded in the negative weights.

3. Discussion

We have examined, for the first time, the premotor cortical functional network that underlies movement generation, using graph-based algorithms that were applied to simultaneously recorded MUAs (from up to 96 channels). We found that movement generation is anticipated by a clear stereotypical increase in synchronization in the form of anti-correlation between several channels and the rest of the network. These channels act as network hubs and are organized in a hierarchical manner. Notably, this phenomenon was not observed for successfully cancelled movements but remained present in trials in which movements where generated despite the command to stop. The latency of the increase in anti-correlation occurs in a window of approximately 200 ms before movement onset. This period is in the same range that is necessary to render a Stop signal effective (the SSRT): if a movement is going to be made, the Stop signal must be presented roughly 200 ms ahead of movement generation to be successful in interrupting the movement. Thus, in stop-correct trials, the effectiveness of the Stop signal is associated with the absence of hubs of anti-correlation.

Our results suggest that the emergence of hubs of anti-correlation can be identified as the neuronal computational strategy the drives the irrevocable maturation of the motor plan. The specific signature in the network topology of the PMd that we detected is characteristic of the pre-movement epoch. Previous studies have shown that before a movement is made, single units, MUA, and LFP in the motor cortices experience strong widespread modulations. They represent the largest change in neuronal activity in delayed reaching tasks (Pani et al., 2014;Pani et al., 2018 Sussillo et al., 2015; Kaufman et al., 2016; Churchland et al., 2012) and as such are believed to correspond to the passage from stable preparation to movement generation. Similar phenomena, compatible with an attractor-like dynamic, have also been observed in the MUA during the same task (Mattia et al., 2013; Marcos et al., 2013). In all of these studies, the latency between the start of the population dynamic and the movement onset is 100–150 ms in a window that is compatible with the anti-correlation patterns that we detected.

In our study, neural activity was recorded at a roughly constant depth (Utah array; electrode length: 1.5 mm). A recent study (Chandrasekaran et al., 2014) found that single unit activity in the PMd is organized following a gradient from superficial to deep layers. Neurons in more superficial layers showed increasing activity during the RT epoch, correlating with behavioural parameters and thus potentially related to decision. Conversely, neurons in deeper layers showed stereotypical modulated activity solely around 150 ms before movement onset. Among these neurons, a subpopulation (approximately 15%) experienced

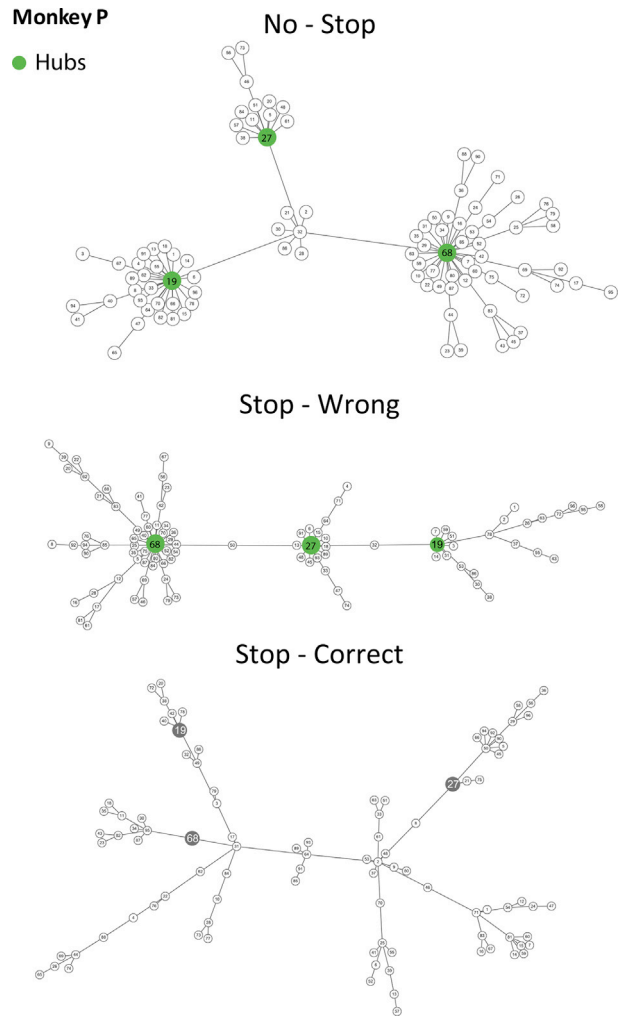

Fig. 7. Minimun spanning tree analysis. Results from Monkey P. MST computed 150 ms before Movement onset for no-stop trials and at the time of the Stop signal presentation for stop-correct and stop-wrong trials. Hubs are indicated by the green circles. Gray circles in stop-correct trials show the location in the MST of the same recording channels.

decreased activity before movement generation. The evidence of anti-correlation between recordings in our study suggests that, thanks to the larger spread of MUA in the cortical layers, we have been able to sample activity from deep layers. However, results also suggest that the location of the tip on the electrodes array is definitively too superficial. In fact, when the network was observed more locally by analyzing single units, the topology was lacking of an organization based on the presence of different populations in anti-correlation.

The MST results suggest that the hubs of anti-correlation that we detected have a function in the computation that is necessary to send the information to subcortical structures. This possibility is supported quantitatively by several groups (Demuru et al., 2013; Dubbelink, 2014) that have recently linked MST changes, based on EEG and MEG data, to cognition and motor functions. Specifically, our results agree with the widespread concept in which most of the traffic in a weighted network flows through the MST. In this scenario, it is not surprising to observe a star-like MST, because this is the optimal configuration for efficient, fast and integrated communication within a network. The cognitive decision of whether to perform a movement is indeed a fast computation, and the command to move could be transferred, through the star-like MST, to lower cortical, subcortical and spinal circuits that will promote muscle activation. Consequently, the information stream would only flow shortly through the hubs, thus helping prevent overloading issues in the network during the ongoing computation (Stam et al., 2014). This, however, does not imply that the PMd is the only region that participates in this form of control. Other cortical and subcortical structures (e.g., basal ganglia, prefrontal cortex) are needed to finalise this process to permit movement initiation (Battaglia-Mayer et al., 2014). Future studies should focus on several crucial aspects: Is the computation that we observed specific at this depth, or is it present across all layers? Do other structures perform similar computations? Is this signature related to specific interactions between the PMd and other brain areas?

In the neural control of movements, various computational strategies have been proposed to define the function of the PMd and MI. In the past several years, many studies have used a dynamical system approach with data from simultaneously recorded neurons. Their main finding is that in motor cortices, neuronal activity evolves smoothly across various state spaces to facilitate movement generation. Importantly, this evolution provides insights into how an entire population of neurons participates in generating movement. This approach gave rise to the idea that several subspaces of neural activity correspond to different behavioural functions. These methods, however, are based on the covariance of the simultaneously recorded neurons and, as such, are suited to account for neuronal activity at the population level, without distinguishing between specific contributions by single neurons (or recording sites) to the topology of the interactions. Our approach differs, because we provide evidence that our computational strategy is based on a hierarchy of hubs. Indeed, this was obtained by considering the mutual interaction between recording sites. By percolation analysis, we succeeded in identifying, without any a priori assumption (in a totally data-driven fashion), the sites that act as hubs. This corresponds to a complete characterization of the topological arrangement of network dynamics, consequently marking a substantial difference from other approaches (e.g., (Churchland et al., 2012; Mattia et al., 2013; Chandrasekaran et al., 2014)). The function of hubs in driving the computation emerges spontaneously from the collective behaviour as an intrinsic property of the system.

To the best of our knowledge, this report is one of the few studies that has performed graph analysis on specific cortical areas at the small scale and mesoscale levels in vivo and during a behavioural task. Schroeter et al. (2015) examined the properties of the primary mouse hippocampal functional network via MUA in vitro, finding that hub neurons have a crucial function in shaping the synchronous dynamics during development. This result confirms the importance of this complex topological structure in coordinating the dynamics at the microcircuit level.

Recently, Dann et al. (2016) — using multielectrode depth cortical recordings — examined the functional topology of three areas of the fronto-parietal network that are involved in grasping, measuring the spiking activity of single units. They found that the network had a modular topology, with hubs in all three areas. Each module was confined primarily to a single area but could also involve neurons in the other areas. Notably, the hubs were composed mainly of oscillatory spiking and synchronized units, whereas the more peripheral units were non-oscillatory. The authors proposed that the oscillator hubs allowed the coordination of functional communication between cortical areas. Further, the topology that they described was highly similar to the that at the whole-brain level using other techniques (EEG, fMRI). In our study, we evaluated the functional topology of a small portion of the cortex: the PMd. Thus, we can not account for the functional communication between the PMd and other areas. Additional study will be necessary to test whether the anti-correlation that we observed is a phenomenon that is limited to the premotor cortex or whether it involves other areas that participate in the cortical reaching network (e.g., parietal regions). In this regard, an important difference between our study and Dann et al. (2016) is that their analysis did not distinguish between positive and negative functional connections.

With our approach, it was possible to determine whether there was synchronization between neural populations and what the sign of this synchrony was. These findings represent an advance in the field, because nearly all previous studies on the motor cortex have merely explored, in

various forms, the nature of positive synchrony (Vaadia et al., 1988; Riehle et al., 1997; Hatsopoulos et al., 1998; Torre, 2016). Renart et al. (2010) and Ecker et al. (2010) provided the first evidence that positive correlations are not the only meaningful associations in micro-neuronal networks. Renart et al. (2010) found that recurrent neural networks can generate an asynchronous state due to fluctuations in the activity of excitatory and inhibitory populations. The authors proposed that the negative correlations that characterize this state prevent uncontrolled network-wide synchrony and facilitate efficient processing of information. Their results were confirmed by in vivo recordings from the somatosensory and auditory cortices of urethane-anesthetized rats. Ecker et al. (2010) analysed neuronal recordings from the primary visual cortex of awake macaques, noting very low spike count correlations between local neurons. They also opined that the decorrelated state of the network might be crucial for hierarchical cortical processing and information routing, offering substantial advantages over communication that relies solely on positive synchrony. Our results are also supported by recent work from Gu et al. (2019), who linked the anatomical and physiological properties of local neural networks through the development of a novel circuit model. They found that highly interconnected hubs neurons emerge as a key feature of the spatiotemporal activity of local cortical circuits. As hypothesized by the authors, the presence of hub neurons in local networks accounts for the transition between dynamic cortical states. Moreover, it provides a solid framework in which the anatomical, functional and dynamic features of brain networks can be integrated. Furthermore, although the attention toward negative weighted links has grown in the past decade, most studies on brain networks have ignored anti-correlations or left them uninterpreted. Has topology that is characterized by strong anti-correlation (as we observed) been reported in large-scale studies by fMRI or EEG? Greicius et al. (2003) made one of the earliest contributions, showing a negative correlation between the default mode network (DMN) and executive function network. Subsequently, anti-correlations have been seen in the attentional network (Fox et al., 2003), sensorial regions (Tian et al., 2007), parietal and medial frontal regions (Tian et al., 2007), the infralimbic cortex (IL) and amygdala (Liang et al., 2012) and in the DMN and executive control network (Di and Biswal, 2013). Further, recent work on fMRI data has focused on the network of negative correlations (Gopinath et al., 2015; Parente et al., 2018; Parente and Colosimo, 2018). Gopinath et al. (2015) examined the anti-correlation maps of healthy patients by resting-state fMRI using a graph-based approach and found that hubs of anti-correlations were involved in important regulatory interactions between various regions, including reciprocal modulations, inhibition and during neurofeedback procedures. They hypothesized that negative links in a brain correlation network are more suitable for describing state-dependent signal couplings than anatomically constrained fluctuations. Parente et al. (2018) reported that central nodes of negative brain networks are affected in schizophrenic patients compared with controls: specifically, patients were characterized by a reduction in centrality measures. The authors speculated that central nodes have an important function in the modulation of other regions that share information with low-degree nodes. These conclusions suggest that, also on the large-scale level, hubs of anti-correlations are likely to be pivotal in cognitive functions.

4. Materials and methods

4.1. Subjects

Two male rhesus macaque monkeys (*Macaca mulatta*), weighing 9 and 9.5 kg, respectively, were used. Animal care, housing, surgical procedures and experiments conformed to European (Directive 86/609/ECC and 2010/63/UE) and Italian (D.L. 116/92 and D.L. 26/2014) laws and were approved by the Italian Ministry of Health. Monkeys were pair-housed with cage enrichment. They were fed daily with standard primate chow that was supplemented with nuts and fresh fruits if necessary. During recording days, the monkeys received their daily water supply during the experiments.

4.2. Apparatus and task

The monkeys were seated in front of a black isoluminant background ($<$0.1 cd/m^2) of a 17-inch touchscreen monitor (LCD, 800 $\times$ 600 resolution), inside a darkened, acoustic-insulated room. A non-commercial software package, CORTEX (http://www.nimh.gov.it), was used to control the presentation of the stimuli and the behavioural responses. Fig. 1 shows the scheme of the general task: a reaching countermanding task (Mirabella et al., 2011). Each trial started with the appearance of a central target (CT) (red circle, diameter 1.9 cm). The monkeys had to reach and hold the CT. After a variable holding time (400–900 ms, 100-ms increments) a peripheral target (PT) (red circle, diameter 1.9 cm) appeared randomly in one of two possible locations, and the CT disappeared (Go signal). In no-stop trials, after the Go signal the subjects had to reach and hold the PT for a variable time (400–800 ms, 100-ms increments) to receive juice. Reaction times (RTs) were defined as the time between the presentation of the Go signal and the onset of the hand movement. In Stop signal trials, the sequence of events was the same until the Go signal. Then, after a variable delay (Stop signal delay, SSD), the CT reappeared (Stop signal), and the monkeys had to hold the CT until the end of the trial (800–1000 ms) to receive the reward (stop-correct trial). Conversely, removing the hand after the Stop signal constituted a wrong response (stop-wrong trial). The same amount of juice was delivered for stop-correct and correct no-stop trials. The intertrial interval was set to 800 ms. Stop trials represented the 25% of all trials in each session. To establish the duration of the SSDs, a staircase tracking procedure was employed. If the monkey succeeded in withholding the response, the SSD increased by one step (100 ms) in the subsequent Stop signal trial. Conversely, if the subject failed, the SSD decreased by one step.

4.3. Extraction and processing of neuronal data

A multielectrode array (Blackrock Microsystems, Salt Lake City) with 96 electrodes (pitch 0.4 mm) was surgically implanted in the left dorsal premotor cortex (PMd; arcuate sulcus and pre-central dimple used as references after opening of the dura; see Supplementary Fig. S 7) to acquire unfiltered electric field potentials (UFP; i.e., the raw signal), sampled at 24.4 kHz (Tucker Davis Technologies, Alachua, FL).

Neuronal activity was recorded from animals fully trained in the task. Since animals were also trained in other motor tasks, we had different sessions with the same task but often separated in time. For the analysis performed in this work we selected one session for each animal were the trial number was sufficiently high and the behaviour was in fully adherence with the expectative of the race model (see 3).

As a measure of neuronal activity at the population level, MUA was extracted offline from the raw signal, as in Mattia et al. (2013), by computing the time-varying power spectra P(ω,t) from the short-time Fourier transform of UFP in 5-ms sliding windows. Relative spectra R(ω,t) were then obtained, normalizing P(ω,t) by their average $P_{ref}(\omega)$ across a fixed window (10–30 min) for the entire recording. The spectrally estimated MUAs are the average R(ω, t) across the ω/2π band [0.2, 1.5] *kHz*. As detailed in Mattia et al. (2013), this estimate relies on two hypotheses.

The first is that high ω components of UFPs result from the convolution of firing rates ν(t) of neurons that are close to the electrode tip with a stereotypical single-unit waveform. R(ω,t) allows one to eliminate the Fourier transform K(ω) of such an unknown waveform, rendering R(ω,t) a good approximation of the ratio of firing rate spectra $|\nu(\omega,t)|^2/|\nu_{ref}(\omega)|^2$

In the second hypothesis, high ω power $|\nu(\omega,t)|^2$ is proportional to the firing rate ν(t) itself (Mattia and Del Giudice, 2002), such that our MUA estimate is proportional to ν(t).

As a last step, logarithmically scaled MUAs were smoothed by a moving average (40-ms sliding window). To analyse single units

correlations we represent neuronal activity via a spike density function (SDF) obtained by convolving the spike train with an exponential function mimicking a postsynaptic potential.

As a convolution function we used the following kernel $K(t)$:

$$K(t) = \left[1 - exp\left(-t / \tau_g\right)\right] \cdot exp(-t / \tau_d) \quad (1)$$

where $\tau_g = 1ms$ corresponds to the growth phase of the synaptic potential, and $\tau_d = 1ms$ to the decay phase (Scangos and Stuphorn, 2010).

For our analysis we selected units that showed an increase/decrease of the average firing rate before movement onset (from −300 ms to movement onset), compared to the 200 ms before Go signal or for at least one movement direction (Wilcoxon rank-sum test $P < 0.01$).

4.4. Preliminary analyses

We first analysed the activity profiles of each recording site. To obtain a uniform view of the changes in MUA levels, we normalised the activity of each channel with respect to its maximum value (see Fig. 2). To examine the local network organization in the PMd, we constructed a functional network that represents the synchronization between the MUAs that were recorded by the electrodes of the array. To this end, we used the Pearson correlation coefficient *C*, because it is one of the best-known methods for calculating synchrony by cross-correlation and because we wanted to focus on the simplest type of relationship between the signals that were recorded from the electrodes: the linear correlation.

For two time series, $X^i(t)$ and $X^j(t)$, at times t, in a 0 lag condition the C_{ij} is calculated as follows:

$$C_{ij} = \frac{Cov[X^i, X^j]}{\sqrt{Var[X^i]Var[X^j]}} \quad (2)$$

$-1 \leq C_{ij} \leq 1$ where high negative values indicate a high inverse linear correlation (anti-synchronization), whereas high positive values reflect a high linear relation between time series (synchronization). For our purposes, $X^i(t)$ is represented by the spectrally estimated MUA in a chosen time window (epoch of analysis: see Fig. 1) of the task, which is usually defined in relation to the behavioural events (e.g., Go Signal, movement onset, etc.). The approach provides an N x N (N = recording sites) correlation matrix, the generic entry of which is the C_{ij} between the *i*-th and *j*-th channel time series in the time window.

We interpreted the correlation matrix as being the adjacency matrix of an undirected weighted graph, in which the nodes are the channels and the weighted edges are the pairwise C_{ij}. Because the purpose of this study was to characterize the network organization that supports the evolution of motor decisions in relation to behavioural events, we needed a graph that represented the time-evolving coupling between electrodes. The simplest route to addressing this issue was to assess the dynamical connectivity between nodes using a sliding window approach to support the static measure of Pearson C_{ij}. To this end, the window width *w* parameter is crucial for segmenting the time series. Because the uncertainty in the correlation measure is given by $\varepsilon = \frac{1}{\sqrt{2B_w W}}$, where B_w is the spectral bandwidth of the data and *w* is the window width (O'Neill et al., 2018), we chose a *w* that effected a good compromise between accurate time resolution and statistical significance. Because MUA lies in the [0.2, 1.5] kHz band, we obtained $\varepsilon \tilde{} 0.06$, choosing $w = 100$ ms.

Once *w* and a step of 5 ms were fixed, we then defined the following task epochs to perform our analysis: for correct no-stop trials and stop-wrong trials, we defined the Go epoch with *w* from −150 ms to +350 ms relative to the Go Signal and the pre-Movement epoch from −350 ms relative to the Movement onset. For correct and stop-wrong trials, we defined the Stop signal epoch, with *w* from −150 ms to +150 ms relative to the Stop signal. Our aim, while using the Stop signal epoch, was to compare conditions in which a movement was generated (stop-wrong trials) to those in which a movement was inhibited (stop-correct trials). This choice is due to the objective of our analyses: inspect the state of the network at the time of the Stop signal presentation and before. Indeed, in agreement with the race model (see 3), a stop trial is wrong if the Stop signal is presented when the motor plan is already at a processing state that it can no longer be inhibited. For this reason, by the time of the Stop signal is presented we expected the network state of stop-wrong trial to differ from the one of stop-correct trials (and comparable to the one of no-stop trials). With our choice of *w*, each time point x_t of the epochs had boundaries of $x_t \pm 50$ ms. Consequently, we managed to fully describe the following intervals: [-100, +300] ms for the Go epoch, [-300, 0] ms for the Pre-Movement epoch and [-100, +100] ms for the Stop signal epoch (see Fig. 1).

To remove noise and outliers from our data, we excluded the trials for which the MUA showed a peak with an amplitude that exceeded the average of the activity of 2 standard deviations in the epochs of interest and for over 80% of the channels from the analysis. Moreover, for Monkey C, damaged electrodes were excluded a priori from the computation, such that its correlation matrix had dimensions of 79 × 79. We computed a correlation matrix for each window of every trial of our epochs to obtain a time course of connectivity at the single-trial level (single-trial network time series). Successively, to generate a unique average matrix for each time window, each coefficient of the single-trial matrices at timestep t was Fisher-transformed, averaged over trials and then back-transformed, ensuring that the variance in C_{ij} was dissociated from its mean (Thompson and Fransson, 2016). As a result, we were able to reconstruct the evolving dynamics of the network as a sequence of snapshots at each time step, at the single-trial and average levels (average network time series).

4.5. Percolation and minimum spanning tree analysis

Fixing an appropriate threshold to study network properties is a common problem when studying brain connectivity matrices (structural or functional) with a graph-based approach. To overcome this obstacle, we adopted a solid method, called percolation. Percolation is a tool that is rooted in statistical physics and has been applied to study phase transitions of connected subgraphs in random networks (Callaway et al., 2000), the first application of which to brain networks was performed by Gallos (Gallos et al., 2012). Since then, the method has been used progressively and successfully to examine the hierarchical organization of brain networks (Nicolini et al., 2017; Vlasov and Bifone, 2017; Mastrandrea et al., 2017; Bordier et al., 2018; Ferraro et al., 2018). We performed percolation analysis to examine the organization of the network without any a priori assumptions (data-driven approach). Simply, percolation consists of the iterative removal of edges of a network and allows one to inspect the intrinsic stability of the network and the presence of a hierarchical organization simultaneously. The usual procedure is to monitor the disaggregation of the network as a function of a threshold of interest (the correlation coefficient, in our case). We used the number of connected components as a parameter to monitor disaggregation (see also Bardella et al., 2016). A hallmark of hierarchical organization is the presence of multiple disaggregation points (more formally, percolation thresholds). At each of these thresholds, the network fractures and reveals its self-organized internal structure, comprising connected subgraphs (Gallos et al., 2012), corresponding to a stepped percolation curve that is endowed with plateaus. Conversely, in a graph with random features (i.e., without organization), the number of connected components is characterized by a sharp transition (Callaway et al., 2000; Albert and Barabasi, 2002). Recent studies (Bordier et al., 2017; Nicolini et al., 2017) have shown that percolation makes it possible to find a threshold that realizes the optimal balance between the removal of spurious correlations that are induced by noise and the loss of information that might be encoded in the weaker links. This threshold is just above the fragmentation of the largest connected component of the graph. Here, although the spurious links have been removed, the connectedness and hence, the structural fundamental characteristics of the network is preserved. Our analysis followed several steps (Bardella

et al., 2016): 1) all experimentally determined correlation coefficients are listed in decreasing/increasing order; 2) starting from the greatest/lowest value, each entry in the list is chosen as a threshold; 3) all links that correspond to the correlations above/below the threshold are removed and 4) the number of connected components that characterize the remaining part of the network is computed. Thus, it is possible to analyse the network of negative and positive correlations. We examined the topology of the functional network of the PMd by inspecting a well-known measure of centrality, the vertex degree. Vertex degree is the number of links to a node i: $VD_i = \sum_{j=1}^{N} c_{ij}$, where c_{ij} is the generic entry of the adjacency matrix. We computed the probability distribution of vertex degrees (i.e. the degree distribution) at the threshold just above the fragmentation of the largest connected component for each step of the average network time series. In the context of complex network theory, nodes that significantly exceeds the average network degree arise as a long tail in the degree distribution and are called hubs (Albert and Barabasi, 2002).

We further studied the topological organization of the functional connections of the PMd by computing the minimum spanning tree (MST). Given an undirected weighted graph, the MST is defined as a unique subgraph that includes all nodes of the original graph and connects them, minimizing the sum of the weights of the edges without forming cycles and minimizing the number of links that are involved. As reported in Stam et al. (2014), in recent years, the use of spanning tree techniques has attracted the interest of neuroscientists, as implemented in EEG (Demuru et al., 2013; Lee et al., 2006, 2010), fMRI (Alexander-Bloch, 2010; Ciftci, 2011; Bardella et al., 2016; Mastrandrea et al., 2017) and magnetoencephalography (MEG) source space data studies (Gong et al., 2009; van Dellen et al., 2009; Dubbelink, 2014). The MST (Mieghem and van Langen, 2005; Mieghem and Magdalena, 2005) provided us with the backbone of the functional interactions in the PMd and allowed us to strengthen the results that were yielded via percolation analysis. We obtained an MST for each step of our average network time series for all epochs. In the MST approach, a tree can have two extreme topologies: path (or chain) and star. In the first case, all nodes are connected to two other nodes, apart from the nodes at either end, each of which have only one link. In the latter, there is one central node that is connected to every other node (leaves) via a single link only. With the star topology, the efficiency of communication and integration of information between nodes is optimal, harbouring the maximum possible number of leaves and the minimum average path length. However, in this topology, the problem of overloading the central node arises easily; thus, the optimal configuration for an efficient tree would be halfway between these two extremes. Between the path and star, there exists a spectrum of many possible configurations, the characteristics of which can be described with a set of relatively simple measures, as detailed in Stam et al. (2014). Among the various measures, we chose the leaf number (LN). The leaf number is the number of nodes with only one link. With the LN, it is possible to intuitively quantify the topology of an MST. A path would have an LN of two, whereas a star of N nodes would have an $LN = N - 1$ that is, the same number of available edges. Thus, an MST that more closely resembles a path will have a lower LN than one that is more similar to a star. A shift from a path-like to star-like configuration of the MST can be interpreted as a change in the network from a less to a more integrated state.

4.6. A statistical benchmark for PMd functional network

To properly assess the statistical significance of percolation and MST analyses, we defined a null model. The choice of a suitable null model remains a complicated issue in network and complex systems science. In this context, in addition to searching for a model that accounts for the observations, one common practice when analysing real-world networks is trying to identify properties that deviate from the null hypothesis, because it is likely that the deviations themselves encode unknown information about the network functions (for an exhaustive review on this topic see Cimini et al., 2019). Conscious of this, the core of our null model consists of an established numerical procedure for correlation matrices (Higham, 2016), which has been used successfully in other studies on brain networks (Bardella et al., 2016; Mastrandrea et al., 2017). Our procedure comprised three steps for each of the epochs under examination: 1) Calculate the empirical probability distributions of the entries of the empirical correlation matrices. Means and standard deviations of the fitted distributions were estimated by maximum-of-the-likelihood procedure. 2) Generate an ensemble of null networks by drawing correlations from the corresponding fitted distributions. We generated an ensemble of 300 synthetic matrices for each matrix of the average network time series. 3) Refine the procedure to compute the nearest correlation matrices to synthetic ones on which to apply our algorithms and compare the results. The last step is likely to be the most delicate, because it requires the procedure from (Higham, 2016) to be implemented, wherein a fast algorithm computes the nearest correlation matrix to a given, symmetric matrix. Indeed, the first two steps alone do not guarantee that true correlation matrices will be obtained: in fact, the synthetic matrices might still have negative eigenvalues. For this reason, most standard randomization techniques are unsuitable. Generally, to be considered a correlation matrix, a matrix must satisfy several requirements: it must be symmetric, with diagonal elements equal to 1, with off-diagonal elements in the range [-1, 1], and it has to be positive semidefinite. With our procedure, we kept the spectrum distribution of the observed correlation matrix fixed, applying random orthogonal similarity transformation — which consisted of repeatedly projecting onto the positive semidefinite matrices and then the unit diagonal matrices — to the diagonal matrix of eigenvalues. This matrix was interpreted, for each epoch, as the weighted adjacency matrix that represented the functional network of the PMd. We then compared the observed percolation trend with those obtained running the procedure on the synthetic matrices. The slope of the percolation curve was computed between correlation values in correspondence of which we detected 2 and n-1 connected components respectively, where n is the number of nodes (we excluded trivial clusters that were represented by the entire network and the single channels/nodes). To test results from MST analysis, the test statistic employed for comparison is the ensemble of LN obtained from the MST computed on the randomized matrices.

Acknowledgment

This work was supported by Sapienza University of Rome, CIDES H2020-2017.

Appendix A. Supplementary data

Supplementary data to this article can be found online at https://doi.org/10.1016/j.neuroimage.2019.116354.

References

Albert, R., Barabasi, A.L., 2002. Statistical mechanics of complex networks. Rev. Mod. Phys. 74, 47–97. https://doi.org/10.1103/RevModPhys.74.47.

Alexander-Bloch, A.F., 2010. Disrupted modularity and local connectivity of brain functional networks in childhood-onset schizophrenia. Front. Syst. Neurosci. 4 https://doi.org/10.3389/fnsys.2010.00147.

Band, G.P., van der Molen, M.W., Logan, G.D., 2003. Horse-race model simulations of the stop-signal procedure. Acta Psychol. 112, S0001691802000793, 105–142.

Bardella, G., Bifone, A., Gabrielli, A., Gozzi, A., Squartini, T., 2016. Hierarchical organization of functional connectivity in the mouse brain: a complex network approach. Sci. Rep. 6, 23060. https://doi.org/10.1038/srep32060.

Battaglia-Mayer, A., Buiatti, T., Caminiti, R., Ferraina, S., Lacquaniti, F., Shallice, T., 2014. Correction and suppression of reaching movements in the cerebral cortex: physiological and neuropsychological aspects. Neurosci. Biobehav. Rev. 42, 232–251. https://doi.org/10.1016/j.neubiorev.2014.03.002.

Bordier, C., Nicolini, C., Bifone, A., 2017. Graph analysis and modularity of brain functional connectivity networks: searching for the optimal threshold. Front. Neurosci. 11 https://doi.org/10.3389/fnins.2017.00441.

Bordier, C., Nicolini, C., Forcellini, G., Bifone, A., 2018. Disrupted modular organization of primary sensory brain areas in schizophrenia. Neuroimage Clin. 18, 682–693. https://doi.org/10.1016/j.nicl.2018.02.035.

Callaway, D.S., Newman, M.E., Strogatz, S.H., Watts, D.J., 2000. Network robustness and fragility: percolation on random graphs. Phys. Rev. Lett. 85, 5468–5471. https://doi.org/10.1103/PhysRevLett.85.5468.

Chandrasekaran, C., Peixoto, D., Newsome, W.T., Shenoy, K.V., 2014. Laminar differences in decision-related neural activity in dorsal premotor cortex. Nat. Commun. 8, 614. https://doi.org/10.1038/s41467-017-00715-0.

Churchland, M.M., Cunningham, J.P., Kaufman, M.T., Foster, J.D., Nuyujukian, P., Ryu, S.I., Shenoy, K.V., 2012. Neural population dynamics during reaching. Nature 487, 51–56. https://doi.org/10.1038/nature11129.

Ciftci, K., 2011. Minimum spanning tree reflects the alterations of the default mode network during Alzheimer's disease. Anesthesiology 113, 11493–11504. https://doi.org/10.1007/s10439-011-0258-9.

Cimini, G., Squartini, T., Saracco, F., Garlaschelli, D., Gabrielli, A., Caldarelli, G., 2019. The statistical physics of real-world networks. Nat. Rev. Phys. 1, 58–71. https://doi.org/10.1038/s42254-018-0002-6.

Colizza, V., Flammini, A., Serrano, M.A., Vespignani, A., 2006. Detecting rich-club ordering in complex networks. Nat. Phys. 2, 110–115. https://doi.org/10.1038/nphys209.

Dann, B., Michaels, J.A., Schaffelhofer, S., Scherberger, H., 2016. Uniting functional network topology and oscillations in the fronto-parietal single unit network of behaving primates. Elife 5. https://doi.org/10.7554/eLife.15719.

van Dellen, E., Douw, L., Hillebrand, A., de Witt Hamer, P.C., Baayen, J.C., Heimans, J.J., Reijneveld, J.C., Stam, C.J., 2009. Epilepsy surgery outcome and functional network alterations in longitudinal MEG: a minimum spanning tree analysis. Neuroimage 86, 354–363. https://doi.org/10.1016/j.neuroimage.2013.10.010.

Demuru, M., Fara, F., Fraschini, M., 2013. Brain network analysis of EEG functional connectivity during imagery hand movements. J. Integr. Neurosci. 12, e70899 https://doi.org/10.1142/S021963521350026X.

Di, X., Biswal, B.B., 2013. Modulatory interactions of resting-state brain functional connectivity. PLoS One 8, e71163. https://doi.org/10.1371/journal.pone.0071163.

Dubbelink, K.T.O., 2014. Disrupted brain network topology in Parkinson's disease: a longitudinal magnetoencephalography study. Brain 127, 197–207. https://doi.org/10.1093/brain/awt316.

Ecker, A.S., Berens, P., Keliris, G.A., Bethge, M., Logothetis, N.K., Tolias, A.S., 2010. Decorrelated neuronal firing in cortical microcircuits. Science 327, 584–586. https://doi.org/10.1126/science.1179867.

Eguiluz, V.M., Chialvo, D.R., Cecchi, G.A., Baliki, M., Apkarian, A.V., 2005. Scale-free brain functional networks. Phys. Rev. Lett. 94, 018102 https://doi.org/10.1103/PhysRevLett.94.018102.

Evarts, V.E., 1968. Relation of pyramidal tract activity to force exerted during voluntary movement. J. Neurophysiol. 31, 14–27. https://doi.org/10.1152/jn.1968.31.1.14.

Ferraro, G.D., Moreno, A., Min, B., Morone, F., Pérez-Ramírez, U., Pérez-Cervera, L., Parra, L.C., Holodny, A., Canals, S., Makse, H.A., 2018. Finding influential nodes for integration in brain networks using optimal percolation theory. Nat. Commun. 9, 2274. https://doi.org/10.1038/s41467-018-04718-3.

Fetz, E., 1992. Are movement parameters recognizably coded in the activity of single neurons? Behav. Brain Sci. 15, 679–690. https://doi.org/10.1017/S0140525X00072599.

Fox, M.D., Zhang, D., Snyder, M.D., Raichle, M.E., 2003. The global signal and observed anticorrelated resting state brain networks. J. Neurophysiol. 101, 3270–3283. https://doi.org/10.1152/jn.90777.2008.

Fujisawa, J., Touyama, H., Hirose, M., 2008. Extracting alpha band modulation during visual spatial attention without flickering stimuli using common spatial pattern. Conf. Proc. IEEE Eng. Med. Biol. Soc. https://doi.org/10.1109/IEMBS.2008.4649229, 620–3.

Gal, E., London, M., Globerson, A., Ramaswamy, S., Reimann, M.W., Muller, E., Markram, H., Segev, I., 2013. Rich cell-type-specific network topology in neocortical microcircuitry. Nat. Neurosci. 20, 1004. https://doi.org/10.1038/nn.4576.

Gallego, J.A., Perich, M.G., Miller, L.E., Solla, S.A., 2017. Neural manifolds for the control of Movement. Neuron 94, 978–984. https://doi.org/10.1016/j.neuron.2017.05.025.

Gallos, L.K., Makse, H.A., Sigman, M., 2012. A small world of weak ties provides optimal global integration of self-similar modules in functional brain networks. Proc. Natl. Acad. Sci. U.S.A. 109, 2825–2830. https://doi.org/10.1073/pnas.1106612109.

Georgopoulos, A.P., Crutcher, M.D., Schwartz, A.B., 1989. Cognitive spatial-motor-processes. 3. Motor cortical prediction of movement direction during an instructed delay period. Exp. Brain Res. 75, 183–194. https://doi.org/10.1007/BF00248541.

Gerhard, F., Pipa, G., Lima, B., Neuenschwander, S., Gerstner, W., 2011. Extraction of network topology from multi-electrode recordings: is there a small-world effect? Front. Comput. Neurosci. 5 https://doi.org/10.3389/fncom.2011.00004.

Gong, P., He, Y., Concha, L., Lebel, C., Gross, D.W., Evans, A.C., Beaulieu, C., 2009. Mapping anatomical connectivity patterns of human cerebral cortex using in vivo diffusion tensor imaging tractography. Cerebr. Cortex 19, 524–536. https://doi.org/10.1093/cercor/bhn102.

Gopinath, K., Krishnamurthy, V., Cabanban, R., Crosson, B.A., 2015. Hubs of anticorrelation in high-resolution resting-state functional connectivity network architecture. Brain Connect. 5 https://doi.org/10.1089/brain.2014.0323, 276–75.

Greicius, M.D., Krasnow, B., Reiss, A.L., Menon, V., 2003. Functional connectivity in the resting brain: a network analysis of the default mode hypothesis. Proc. Natl. Acad. Sci. U.S.A. 100, 253–258. https://doi.org/10.1073/pnas.0135058100.

Gu, Y., Qi, Y., Gong, P., 2019. Rich-club connectivity, diverse population coupling, and dynamical activity patterns emerging from local cortical circuits. PLoS Comput. Biol. 15, e1006902 https://doi.org/10.1371/journal.pcbi.1006902.

Hatsopoulos, N.G., Ojakangas, C.L., Paninski, L., Donoghue, J.P., 1998. Information about movement direction obtained from synchronous activity of motor cortical neurons. Proc. Natl. Acad. Sci. U.S.A. 95, 15706–15711. https://doi.org/10.1073/pnas.95.26.15706.

Higham, N.J., 2016. Computing the nearest correlation matrix - a problem from finance. IMA J. Numer. Anal. 22 https://doi.org/10.1038/s42254-018-0002-6, 392–343.

Kaufman, M.T., Seely, J.S., Sussillo, D., Ryu, S.I., Shenoy, K.V., Churchland, M.M., 2016. The largest response component in the motor cortex reflects movement timing but not movement type. eNeuro 3.

Kiani, R., Cueva, C.J., Reppas, J.B., Peixoto, D., Ryu, S.I., Newsome, W.T., 2015. Natural grouping of neural responses reveals spatially segregated clusters in prearcuate cortex. Neuron 85, 1359–1373. https://doi.org/10.1016/j.neuron.2015.02.014.

Konig, P., Engel, A.K., 1995. Correlated firing in sensory-motor systems. Curr. Opin. Neurobiol. 5, 511–519. https://doi.org/10.1016/0959-4388(95)80013-1.

Lara, A.H., Cunningham, J.P., Churchland, M.M., 2018. Different population dynamics in the supplementary motor area and motor cortex during reaching. Front. Behav. Neurosci. 9, 2754. https://doi.org/10.1038/s41467-018-05146-z.

Lee, U., Kim, S., Jung, K.Y., 2006. Classification of epilepsy types through global network analysis of scalp electroencephalograms. Phys. Rev. E - Stat. Nonlinear Soft Matter Phys. 73, 041920 https://doi.org/10.1103/physreve.73.041920.

Lee, U., Oh, G., Kim, S., Noh, G., Choi, B., Mashour, G.A., 2010. Brain networks maintain a scale-free organization across consciousness, anesthesia, and recovery: evidence for adaptive reconfiguration. Anesthesiology 113, 1081–1091. https://doi.org/10.1097/ALN.0b013e3181f229b5.

Liang, Z., King, J., Zhang, N., 2012. Anticorrelated resting-state functional connectivity in awake rat brain. Neuroimage 59, 1190–1199. https://doi.org/10.1016/j.neuroimage.2011.08.009.

Liégeois, R., Ziegler, E., Phillipsand, C., Geurts, P., Gómez, F., Bahri, M.A., Yeo, B.T., Soddu, A., Vanhaudenhuyse, A., Laureys, S., Sepulchre, R., 2014. Cerebral functional connectivity periodically (de)synchronizes with anatomical constraints. Brain Struct. Funct. 221, 2985–2997. https://doi.org/10.1007/s00429-015-1083-y.

Logan, G.D., Cowan, W.B., Davis, K.A., 1984. On the ability to inhibit simple and choice reaction time responses: a model and a method. J. Exp. Psychol. Hum. Percept. Perform. 10, 276–291. https://doi.org/10.1037//0096-1523.10.2.276.

Luca, M.D., Beckmanna, C.F., Stefano, N.D., Matthews, P.M., Smith, S.M., 2006. fMRI resting state networks define distinct modes of long-distance interactions in the human brain. Neuroimage 8, 1359–1367. https://doi.org/10.1016/j.neuroimage.2005.08.035.

Lutcke, H., Gerhard, F., Zenke, F., Gerstner, W., Helmchen, F., 2013. Inference of neuronal network spike dynamics and topology from calcium imaging data. Front. Neural Circuits 7. https://doi.org/10.3389/fncir.2013.00201.

Marcos, E., Pani, P., Brunamonti, E., Deco, G., Ferraina, S., Verschure, P., 2013. Neural variability in premotor cortex is modulated by trial history and predicts behavioral performance. Neuron 78, 249–255. https://doi.org/10.1016/j.neuron.2013.02.006.

Mastrandrea, R., Gabrielli, A., Piras, F., Spalletta, G., Caldarelli, G., Gili, T., 2017. Organization and hierarchy of the human functional brain network lead to a chain-like core. Sci. Rep. 7, 4888. https://doi.org/10.1038/s41598-017-04716-3.

Mattia, M., Del Giudice, P., 2002. Population dynamics of interacting spiking neurons. Phys Rev E. 66 https://doi.org/10.1103/PhysRevE.66.051917.

Mattia, M., Ferraina, S., Del Giudice, P., 2010. Dissociated multi-unit activity and local field potentials: a theory inspired analysis of a motor decision task. Neuroimage 3, 812–823. https://doi.org/10.1016/j.neuroimage.2010.01.063.

Mattia, M., Pani, P., Mirabella, G., Costa, S., Del Giudice, P., Ferraina, S., 2013. Heterogeneous attractor cell assemblies for motor planning in premotor cortex. J. Neurosci. 33, 11155–11168. https://doi.org/10.1523/JNEUROSCI.4664-12.2013.

Michaels, J.A., Dann, B., Scherberger, H., 2016. Neural population dynamics during reaching are better explained by a dynamical system than representational tuning. PLoS Comput. Biol. 12, e1005175 https://doi.org/10.1371/journal.pcbi.1005175.

Mieghem, P.V., van Langen, S., 2005. Influence of the link weight structure on the shortest path. Phys. Rev. E - Stat. Nonlinear Soft Matter Phys. 71, 056113 https://doi.org/10.1103/PhysRevE.71.056113.

Mieghem, P.V., Magdalena, S.M., 2005. Phase transition in the link weight structure of networks. Phys. Rev. E - Stat. Nonlinear Soft Matter Phys. 72, 056138 https://doi.org/10.1016/j.neuroimage.2013.10.010.

Mirabella, G., Pani, P., Ferraina, S., 2011. Neural correlates of cognitive control of reaching movements in the dorsal premotor cortex of rhesus monkeys. J. Neurophysiol. 106, 1454–1466. https://doi.org/10.1152/jn.00995.2010.

Nicolini, C., Bordier, C., Bifone, A., 2017. Community detection in weighted brain connectivity networks beyond the resolution limit. Neuroimage 28, 39. https://doi.org/10.1016/j.neuroimage.2016.11.026.

O'Neill, G.C., Tewarie, P., Vidaurre, D., Liuzzi, L., Woolrich, M.W., Brookes, M.J., 2018. Dynamics of large-scale electrophysiological networks: a technical review. Neuroimage 180, 559–576. https://doi.org/10.1016/j.neuroimage.2017.10.003.

Pani, P., Bello, F.D., Brunamonti, E., D'Andrea, V., Papazachariadis, G., Ferraina, S., 2014. Alpha- and beta-band oscillations subserve different processes in reactive control of limb movements. Front. Behav. Neurosci. 8 https://doi.org/10.3389/fnbeh.2014.00383.

Pani, P., Giarrocco, F., Giamundo, M., Montanari, R., Brunamonti, E., Ferraina, S., 2018. Visual salience of the stop signal affects the neuronal dynamics of controlled inhibition. Scientific Reports 8(1):14265. https://doi.org/10.1038/s41598-018-32669-8.

Parente, F., Colosimo, A., 2018. Anticorrelations between active brain regions: an agent-based model simulation study. Neural Plast. 6815040 https://doi.org/10.1155/2018/6815040.

Parente, F., Frascarelli, M., Mirigliani, A., Fabio, F.D., Biondi, M., Colosimo, A., 2018. Negative functional brain networks. Imag. Behav. 12, 467–476. https://doi.org/10.1007/s11682-017-9715-x.

Power, J.D., Schlaggar, B.L., Lessov-Schlaggar, C.N., Petersen, S.E., 2013. Evidence for hubs in human functional brain networks. Neuron 79, 798–813. https://doi.org/10.1016/j.neuron.2013.07.035.

Renart, A., de la Rocha, J., Bartho, P., Hollender, L., Parga, N., Reyes, A., Harris, K.D., 2010. The Asynchronous state in cortical circuits. Science 327, 587–590. https://doi.org/10.1126/science.1179850.

Riehle, A., Grün, S., Diesmann, M., Aertsen, M., 1997. Spike synchronization and rate modulation differentially involved in motor cortical function. Science 278, 1950–1953. https://doi.org/10.1126/science.278.5345.1950.

Scangos, K.W., Stuphorn, V., 2010. Medial frontal cortex motivates but does not control movement initiation in the countermanding task. J. Neurosci. 3, 1968–1982. https://doi.org/10.1523/JNEUROSCI.4509-09.2010.

Schroeter, M.S., Charlesworth, P., Kitzbichler, M.G., Paulsen, O., Bullmore, E.T., 2015. Emergence of rich-club topology and coordinated dynamics in development of hippocampal functional networks in vitro. J. Neurosci. 35, 5459–5470. https://doi.org/10.1523/JNEUROSCI.4259-14.2015.

Shenoy, K.V., Sahani, M., Churchland, M.M., 2012. Cortical control of arm movements: a dynamical systems perspective. Annu. Rev. Neurosci. 36, 337–359. https://doi.org/10.1146/annurev-neuro-062111-150509.

Shin, J., Mashour, G.A., Ku, S., Kim, S., Lee, U., 2013. Subgraph "backbone" analysis of dynamic brain networks during consciousness and anesthesia. PLoS One 8, e70899. https://doi.org/10.1371/journal.pone.0070899.

Sporns, O., Honey, C.J., Kötter, R., 2007. Identification and classification of hubs in brain networks. PLoS One 2, e1049. https://doi.org/10.1371/journal.pone.0001049.

Stam, C., Tewarie, P., Dellen, E.V., van Straaten, E., Hillebrand, A., Mieghem, P.V., 2014. The trees and the forest: characterization of complex brain networks with minimum spanning trees. Int. J. Psychophysiol. 92, 129–138. https://doi.org/10.1016/j.ijpsycho.2014.04.001.

Sussillo, D., Churchland, M.M., Kaufman, M.T., Shenoy, K.V., 2015. A neural network that finds a naturalistic solution for the production of muscle activity. Nat. Neurosci. 18, 1025–1033. https://doi.org/10.1038/nn.4042.

Thompson, W.H., Fransson, P., 2016. On stabilizing the variance of dynamic functional brain connectivity time series. Brain Connect. 6, 735–746. https://doi.org/10.1089/brain.2016.0454.

Tian, L., Jiang, T., Liu, Y., Yu, C., Wang, K., Zhou, Y., Song, M., Li, K., 2007. The relationship within and between the extrinsic and intrinsic systems indicated by resting state correlational patterns of sensory cortices. Neuroimage 36, 684–690. https://doi.org/10.1152/jn.90777.2008.

Torre, E., 2016. Spike synchronization and rate modulation differentially involved in motor cortical function. J. Neurosci. 36, 8329. https://doi.org/10.1523/JNEUROSCI.4375-15.2016.

Vaadia, E., Kurata, K., Wise, S.P., 1988. Neuronal activity preceding directional and nondirectional cues in the premotor cortex of rhesus monkeys. Somatosens. Mot. Res. 6, 207–230. https://doi.org/10.3109/08990228809144674.

Vlasov, V., Bifone, A., 2017. Hub-driven remote synchronization in brain networks. Sci. Rep. 1, 10403. https://doi.org/10.1038/s41598-017-09887-7.

Wise, S.P., Boussaoud, D., Johnson, P.B., Caminiti, R., 1997. Premotor and parietal cortex: corticocortical connectivity and combinatorial computations. Annu. Rev. Neurosci. 20, 25–42. https://doi.org/10.1146/annurev.neuro.20.1.25.

Yu, S., Huang, V., Singer, W., Nikolic, D., 2006. A small world of neuronal synchrony. Cerebr. Cortex 18, 2891–9012. https://doi.org/10.1093/cercor/bhn047.